Chemical Papers (2020) 74:229–238
https://doi.org/10.1007/s11696-019-00874-y

ORIGINAL PAPER

Facile development of highly sensitive femtomolar electrochemical DNA biosensor using gold nanoneedle-modified electrode

S. Rafique[1] · S. Khan[1] · S. Bashir[2] · R. Nasir[1]

Received: 25 April 2019 / Accepted: 8 July 2019 / Published online: 15 July 2019

Abstract

In this paper, a simple one-step electrochemical method was employed for the deposition of gold nanostructures. Different morphologies (Au-nanorods and Au-nanoneedles) were obtained using different concentrations of gold chloride ($HAuCl_4 \cdot 3H_2O$) solution. The gold nanostructure-modified surface was used for the fabrication of DNA biosensor, which was characterized by cyclic voltammetry and differential pulse voltammetry. The DNA immobilization and hybridization on Au-nanorods and Au-nanoneedles showed a detection limit of 10 fM and 0.2 fM, respectively, with wide dynamic range of 0.2 fM to 10 nM. The Au-nanoneedle electrode showed improved detection limit, which is fifty times lower than that of the Au-nanorods. The electrochemical DNA biosensor showed a good selectivity and sensitivity towards the detection of target DNA. The enhancement in response of DNA biosensor would be an exciting addition in clinical diagnosis due to an improved detection limit.

Keywords Gold nanostructures · Electrodeposition · DNA immobilization · DNA hybridization · Electrochemical DNA biosensor

Introduction

Recently, biosensors have received a great interest due to their potential applications in different fields of medicine, industry, food, environmental and agriculture. The developed biosensors showed highly sensitive and selective response in clinical diagnosis (Janegitz et al. 2014), DNA damage (Hajkova et al. 2017; Hlavata et al. 2012) gene detection (Povedano et al. 2018), genetic disorder (Lee et al. 2017; Fojta et al. 2016), and several biomarker detection (Sohrabi et al. 2016; Huang et al. 2017) among many other applications. The biosensors are easy to prepare with low cost and high selectivity. These promising characteristics of biosensor make it a potential candidate in the advancement of our health care systems.

The recent development of DNA biosensor is strongly dependent on its performance which requires optimal orientation of DNA, immobilization of DNA probe, and spacing for target DNA hybridization (Saeed et al. 2017). Some probe DNA with enzyme or redox molecules are used for hybridization detection confirmation. Nowadays, different nanomaterials such as carbon nanotubes (Rasheed and Sandhyarani 2017; Jiang and Lee 2018; Fortunati et al. 2019), gold nanoparticle (Alim et al. 2018; Hun et al. 2017), quantum dots (Kokkinos et al. 2015), and silver nanoparticles (Huang et al. 2014) are being employed for DNA immobilization and confirmation of DNA attachment on sensor surface.

The nanomaterials have been used to improve sensitivity and signal of DNA biosensor. Among these nanomaterials, gold nanostructures (Au nanostructures) are strong candidates due to their unique optical and mechanical properties, along with good chemical stability (Mohammed et al. 2014; Nakano et al. 2014; Soleymani et al. 2009, 2011). There are several methods for the synthesis of Au nanostructures. However, the electrochemical synthesis of Au nanostructures has been extensively used due to its advantage over chemical synthesis such as size, shape, morphology, and growth rate that can be well controlled

✉ S. Rafique
saima.rafique@mail.au.edu.pk

[1] Department of Physics, Air University, PAF Complex, E-9, Islamabad 44000, Pakistan

[2] Department of Physics and Applied Mathematics, Pakistan Institute of Engineering and Applied Sciences, Islamabad 45650, Pakistan

by deposition potential, current densities and salt concentrations (Li et al. 2013). Fu et al. (2016) has developed a novel electrochemical immunosensing protocol for neuron-specific enolase (NSF, as a model analyte) by the use of gold nanostructures. They have electrodeposited the gold nanoflowers on electrode and observed the enhancement in sensitivity towards NSF detection. Similarly, Mogha et al. (2018) has developed gold nanoparticles based DNA biosensor for mycobacterium tuberculosis. Their work indicated that the high detection efficiency of 0.1 fM and high specificity (92%) to mycobacterium tuberculosis target DNA by the use of gold nanoparticles of 6 nm diameter. Liu et al. (2010) has also developed simple strategy of electroless deposition for gold nanoparticle (AuNP) modification on the conductive substrate. They observed the enhancement in immobilization and hybridization of gold nanoparticles, along with the increase in detection limit to about three orders of magnitude. A high surface coverage and different shapes of Au nanostructures were obtained in less time by electrochemical methods compared to the other methods (Elahi et al. 2018; Li et al. 2013). These electrochemically synthesized Au nanostructures of different shapes make them a versatile tool for different applications such as DNA bio-sensing (Tan et al. 2014).

In this work, we have investigated the effect of gold chloride ($HAuCl_4{\cdot}3H_2O$) concentration on morphology of gold nanostructures. The aim is to examine the electrochemical properties of the interfaces and the physical state of gold faces. The gold nanostructures were prepared by simple electrochemical method and changing the gold ion concentration. These electrochemical synthesized structures are further used for the fabrication of DNA biosensor. Furthermore, the dependence of structure morphology on efficiency of DNA hybridization was examined. The Au-nanoneedle nanostructures showed an excellent capability of DNA immobilization and hybridization. The fabricated electrochemical DNA biosensor shows a high selectivity using ruthenium hexamine $[Ru(NH_3)_6]^{3+}$ as an electroactive complex and sensitivity towards the detection of target DNA (Zhong et al. 2012). A detection limit of 0.2 fM towards target DNA can be achieved. The currently developed methodology of electrode modification can also be employed for protein and enzyme biosensors.

Experimental

Materials and chemicals

The thiol-labelled DNA (IS1002) was commercially synthesized from Sure Bio-Diagnostics and Pharmaceuticals with the base sequence as follows:

1. 5′-SH-TTCAGGCACACAAACTTGATGGGCG-3′ (sequence 1)
2. 5′-CGCCCATCAAGTTTGTGTGCCTGAA-3′ (complementary target DNA sequence of 1)
3. 5′-AGACTAATCCATACTGATAAGATCC-3′ (non-complementary target DNA sequence)

where SH-5′ refers to $HO_3PO\text{-}(CH_2)_6\text{-}SS\text{-}(CH_2)_6\text{-}OH$.

The chemicals used for the synthesis of gold nanostructures (Au nanostructures) were hydrogen tetrachloroaurate (III) trihydrate ($HAuCl_4{\cdot}3H_2O$) and perchloric acid ($HClO_4$) (Sigma-Aldrich). The hexaammineruthenium (III) chloride (RuHex) and 6-mercapto-1-hexanol (MCH) used for electrochemical study and DNA hybridization were purchased from Sigma-Aldrich. All chemicals used in this experiment are of analytical grade and all solutions employed were prepared in milli-Q water. The glassware were autoclaved before using them for the preparation of DNA biosensor.

Apparatus

Electrochemical impedance, cyclic voltammetry and differential pulse voltammetry (DPV) were performed on CHI760D (CH Instruments, USA) electrochemical workstation. A conventional three-electrode cell, a working gold electrode (CHI101, diameter 2.0 mm), platinum auxiliary electrode (CHI102, diameter 2.0 mm) and silver/silver chloride reference electrode (CHI111, 3 M KCl), was used. Electrochemical measurements were performed in 10-ml glass cell. The electrochemical data for differential pulse voltammetry were collected with pulse amplitude of 50 mV, pulse width 50 ms, pulse period 200 ms which was recorded in the potential window of − 0.06 V to − 0.45 V with increment of 0.001 V vs. Ag/AgCl at scan rate of 20 mV s^{-1} with current sampling for the last 20 ms. Ag/AgCl at scan rate of 20 mV s^{-1}. Cyclic voltammetry was performed between 0 and 0.4 V at scan rate 50 mV s^{-1} and potential step of 5 mV was used to assess the response of electrode. Electrodes were also characterised using electrochemical impedance spectroscopy (EIS). The EIS response was measured at ambient temperature, at polarization potential of 0.208 V in frequency range of 100 kHz and 0.1 Hz with amplitude of 10 mV, and the impedance spectra were fitted to a Randles equivalent circuit to determine the charge transfer resistance. All electrochemical measurements were performed in 1 mM hexaammineruthenium (III) chloride mixed in 0.1 M KCl solution (RuHex). All measurements were taken immediately after adding the reagents to the solution.

The atomic force microscope (SPM 3100, Veeco Instruments, Inc. and JEOLJEM-2100) and field emission scanning electron microscopy (FESEM) were used to study the surface morphology of gold nanostructures. X-ray diffraction (XRD) was performed on an X'Pert Pro X-ray diffractometer

(PANALYTICAL Xpert Pro) which was operated at a voltage of 40 kV and a current of 30 mA with CuKα radiation.

Gold nanostructure preparation

The synthesis of gold nanostructures (Au nanostructures) was carried out via an electrochemical oxidation/reduction in a simple three-electrode glass electrolysis cell schematic shown in Fig. 1. Initially, gold electrodes were polished with 1 µm and 0.05 µm alumina powder followed by ultrasonic cleaning in acetone and water. Electrochemical pre-treatment measurements were performed in H_2SO_4 (0.5 M) until stable cyclic voltammogram was obtained. The electrode was then dried at room temperature. Gold nanostructures were electrodeposited on clean plain electrode at a potential of − 0.08 V using 4 mM and 15 mM concentration of gold chloride as shown in step 1 of Fig. 1 (Mahshid et al. 2016; Tian et al. 2006).

DNA biosensor fabrication

The thiolated DNA was immobilized on electrode which was modified with gold nanostructures using 2 µM DNA sequence 1 (probe DNA) in phosphate buffer solution (0.1 M). The Au nanostructure-modified electrode was dipped in probe DNA solution for 12 h in step 2. The non-specifically adsorbed DNA was then removed by incubating electrode in blank PBS solution for 1 h. The Au nanostructure/probe DNA electrode was further treated with 1 mM MCH to obtain a good orientation of probe DNA (Veselinovic et al. 2018). The electrode was washed afterwards with PBS and deionized water and dried with argon gas. In step 3, the probe-modified electrode was immersed in solution having different concentration of target DNA (complementary and non-complementary) in PerfectHyb Plus hybridization buffer (1×) (Sigma-Aldrich), for 1 h at room temperature to obtain the maximum strand displacement on the surface. Finally, the electrode was rigorously washed with PBS and water to remove physically adsorbed DNA. The limit of detection (LOD) was calculated as the DNA concentration corresponding to a threefold of standard deviation of blank solution (Hajkova et al. 2015). The parameters of calibration curves were obtained from the origin Pro. 2015 software.

Results and discussion

Surface morphology

Surface morphological analysis of Au nanostructures synthesized by electrochemical technique was performed by FESEM as shown in Fig. 2. The effect of varying concentration of gold chloride is shown in Fig. 2a–c. Figure 2a shows the gold film sputtered on silicon surface. It shows a smooth surface of gold forming small islands distributed uniformly all over the sample. However, the two different concentrations reveal two different structure morphologies. At low concentration of 4 mM, the overall morphology features show a rod-like structure formed of diameter in the range of 100–120 nm. At fourfold higher concentration of gold chloride, a remarkable difference in morphology appeared as compared to the one obtained for 4 mM concentration. The structures are appeared to be needle-like instead of rods and are found to be fewer as compared to Au-nanorods. When the concentration of gold chloride increased to 15 mM, these needle-like structures showed a series of peaks and valleys. These needles were ridge and had inconsistent shape. This suggested that the concentration of gold ions play a critical role in the kinetics of nanostructure formation. Interestingly, higher gold ion concentrations did not create a greater abundance of needles but rather promote thicker and smoother shapes.

The average length, width and the aspect ratio were calculated for Au nanostructures at varying concentrations of gold chloride solution. Au-nanorods with average length of 207 ± 4 nm having an average diameter of 105 ± 2 nm for 4 mM concentration with aspect ratios (length/width) 1.97 were formed in significant amount. Furthermore, the increase in concentration from 4 mM to 15 mM has reduced

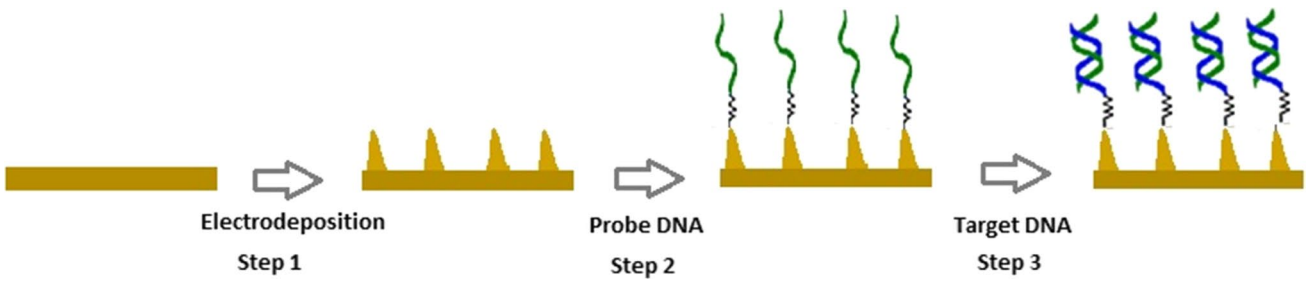

Fig. 1 Schematics of preparation of DNA biosensor, step 1: electrodeposition of gold nanostructures using different concentrations of gold chloride, step 2: immobilization of probe DNA, step 3: attachment of target DNA (complementary and non-complementary) sequence

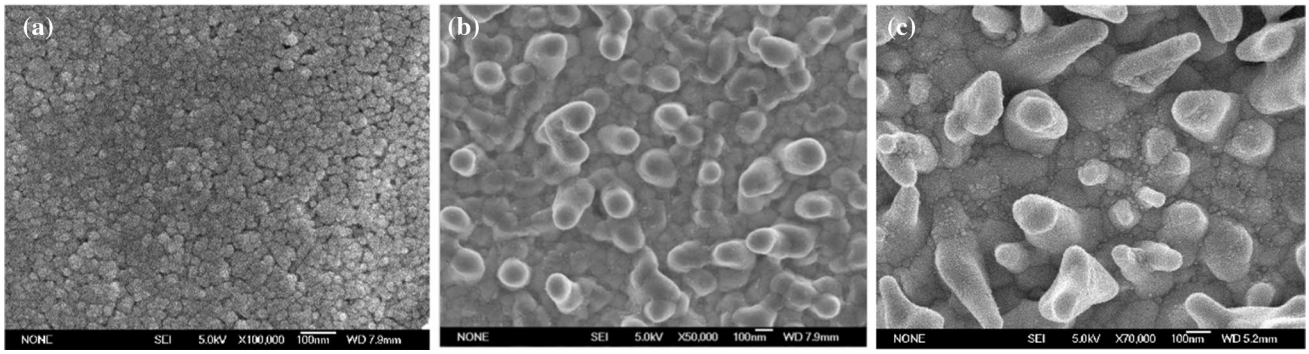

Fig. 2 FESEM micrograph of Au nanostructures. **a** Sputtered gold film, **b** Au-nanorods with 4 mM concentration, **c** Au-nanoneedles with 15 mM concentration of gold chloride ($HAuCl_4 \cdot 3H_2O$)

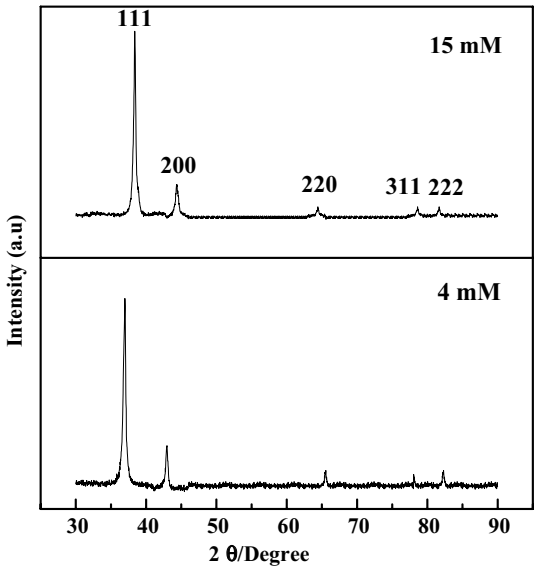

Fig. 3 XRD patterns of the gold nanorod and nanoneedles for 4 mM (bottom) and 15 mM (top) gold chloride concentrations

length of nanorods while increased their diameters. As a result, the aspect ratio was decreased by a factor of 3.75. The Au-nanoneedles became thicker and shorter resulting in an increase in aspect ratio and hence Au-nanorods emerged as a high-quality Au-nanoneedle.

Structural analysis

Gold nanostructure formation is monitored by X-ray diffractometry (XRD). To study the structural properties of synthesized Au nanostructures, X-ray diffraction spectroscopy (XRD) was performed. Figure 3 shows the XRD patterns of Au-nanorods with 4 mM (bottom), and Au nanoneedles with 15 mM (top) gold chloride concentration-dependent Au nanostructures. The major diffraction peaks observed were (111), (200), (220), (311) and (222). The ratio of the diffraction peaks (111) and (200) is found to be very small. It confirms that Au-nanorods and Au-nanoneedles were dominated by (111) face. Thus, (111) planes tend to be preferentially oriented parallel to the surface of the supporting substrate. Therefore, the Au nanostructure (which was electrochemically synthesized) was composed of pure crystalline gold with face-cantered cubic (fcc) structure (Sun et al. 2004). This sharp peak indicates the crystalline nature of Au nanostructures.

Cyclic voltammetry (CV) was performed to investigate the surface state at the metal–solution interface, and surface area of planar and nanostructured gold electrode. It established a relationship between concentration-dependent surface structures with XRD technique. In acidic solution, different gold faces show different CV (Hamelin 1996). The concentration-dependent CV was performed in 0.01 M solution of H_2SO_4. The results are shown in Fig. 4. It is interesting to note that the oxidation peak was around + 1.3 V in Fig. 4b, c, respectively, which is a characteristic of gold (111) face (Tian et al. 2006). A small oxidation peak around + 1.1 V was also observed. This peak represents the presence of gold (100) or (110) faces. However, Fig. 4a represents the CV of sputtered gold film. The peak with (111) face was much less prominent than the peak observed in case of rod-like and needle-like gold nanostructures. These results are in agreement with the above presented XRD data. Therefore, it can be concluded that (111) face was most stable among all other faces present in Au nanostructures.

Surface area of Au nanostructured electrode

The relative surface area of the sputtered gold film and Au nanostructures electrochemically deposited on electrode can be evaluated by columbic integration of reduction peak (Park et al. 2011). The relative surface area of gold electrode can be evaluated based on the area integration. The relative surface area of the planar electrode with nanostructured electrode is 1:2.7 for 4 mM concentration. However,

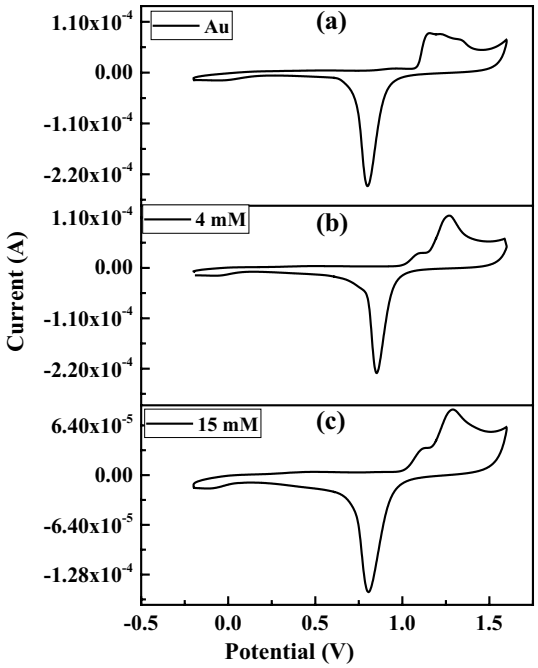

Fig. 4 Characterization of gold electrode with cyclic voltammogram obtained at the scan rate of 50 mV s^{-1} in 0.01 M aqueous H_2SO_4 for **a** sputtered gold surface, **b** 4 mM, and **c** 15 mM gold chloride concentrations

the relative surface area was 1:3.6 for 15 mM concentration. This enhancement in surface area for modified electrodes showed a prominent effect on the performance of DNA biosensor.

Electrochemical behaviour of Au nanostructured electrode

Cyclic voltammetry

The electron transfer through hexaammineruthenium (III) chloride (RuHex) was used to monitor at different step of DNA biosensor preparation process as shown in Fig. 5a, b. Figure 5a represents the CV obtained for different steps of preparation of DNA biosensor on Au-nanorod electrode. While Fig. 5b constitutes the changes in current observed for biosensor preparation on Au-nanoneedle surface. The measurements were performed on electrodes at the scan rate of 50 mV s^{-1}. It can be seen that well-defined peaks of anode (E_{pa}) and cathode (E_{pc}) at a potential of 0.17 V and 0.23 V, respectively, were observed for planar gold (Au) electrode (black line). After deposition of Au-nanorods and Au-nanoneedles, the peak current increased and a peak-to-peak potential separation showed decrement. This indicates a better electrochemical behaviour at electrode surface. In both cases, Au-nanorods and Au-nanoneedles, a decrease in current was observed by immobilization of thiolated DNA (Probe DNA). This suggested that the electrode had been successfully modified with probe DNA. Furthermore, a decrease in current was observed after DNA hybridization of probe DNA and target complementary DNA (pink line). The potential separation $\Delta E_p = E_{pc} - E_{pa}$ was also evaluated. The peak-to-peak potential separation came out to be 0.0703 V for planar Au surface. After the deposition of Au-nanorods and Au-nanoneedles, this separation was decreased to 0.0599 and 0.0584, respectively, which suggest that the voltammetric response strongly depends on the surface area. It also indicates an increase in the electrochemical reversibility of RuHex reactions at the nanostructured electrode surface. The peak current drops from 10.1 to 7.7 µA and 11.6 to 9.5 µA for Au-nanorods and Au-nanoneedles, respectively, with the immobilization of DNA. A further increase in potential separation of 0.0623, 0.0812 V and 0.0670, 0.0875 V was observed after immobilization of thiolated DNA, and complementary DNA on Au-nanorods and Au-nanoneedles electrodes, respectively. This describes an improved adhesion of DNA on nanostructured electrodes and good reversibility of the nanostructured electrodes.

Impedance measurement

Impedance measurement (EIS) provides information occurring on the electrode surface. This leads to an impedance measurement of the Au nanostructures which were performed in the frequency range of 1 Hz–10 kHz. The EIS plot shown in Fig. 5c, d consists of two regions. One is semi-circular part in high-frequency regime and the other is straight line in low-frequency regime. The semi-circular part corresponds to the charge transfer resistance R_{ct} between the electrode and the electrolyte solution. Also, its intercept at high frequency on real axis corresponds to electrolyte resistance (R_s). The straight line corresponds to the diffusion-limited process at low frequency representing the Warburg impedance (W). Figure 5c, d represents the Nyquist plot of differently modified electrode. In both cases, the planar gold electrode showed a smaller semicircle with R_{ct} value of about 700 Ω (black curve). After modification with Au-nanorods and Au-nanoneedles, it almost became a straight line indicating an improvement in electron transfer. The R_{ct} value was further increased to 1100 and 1500 Ω after immobilization of probe and target DNA, respectively, in case of Au-nanorod-modified electrode. However, a prominent change in R_{ct} value was observed for Au-nanoneedle-modified electrode. The R_{ct} value obtained was 2400 Ω and 3500 Ω, respectively, after immobilization of probe and target DNA, respectively. This suggests that Au-nanoneedles exhibit larger surface area which in turn showed enhanced attachment of probe DNA on electrode surface. The results indicate that the EIS is an excellent tool to monitor the DNA

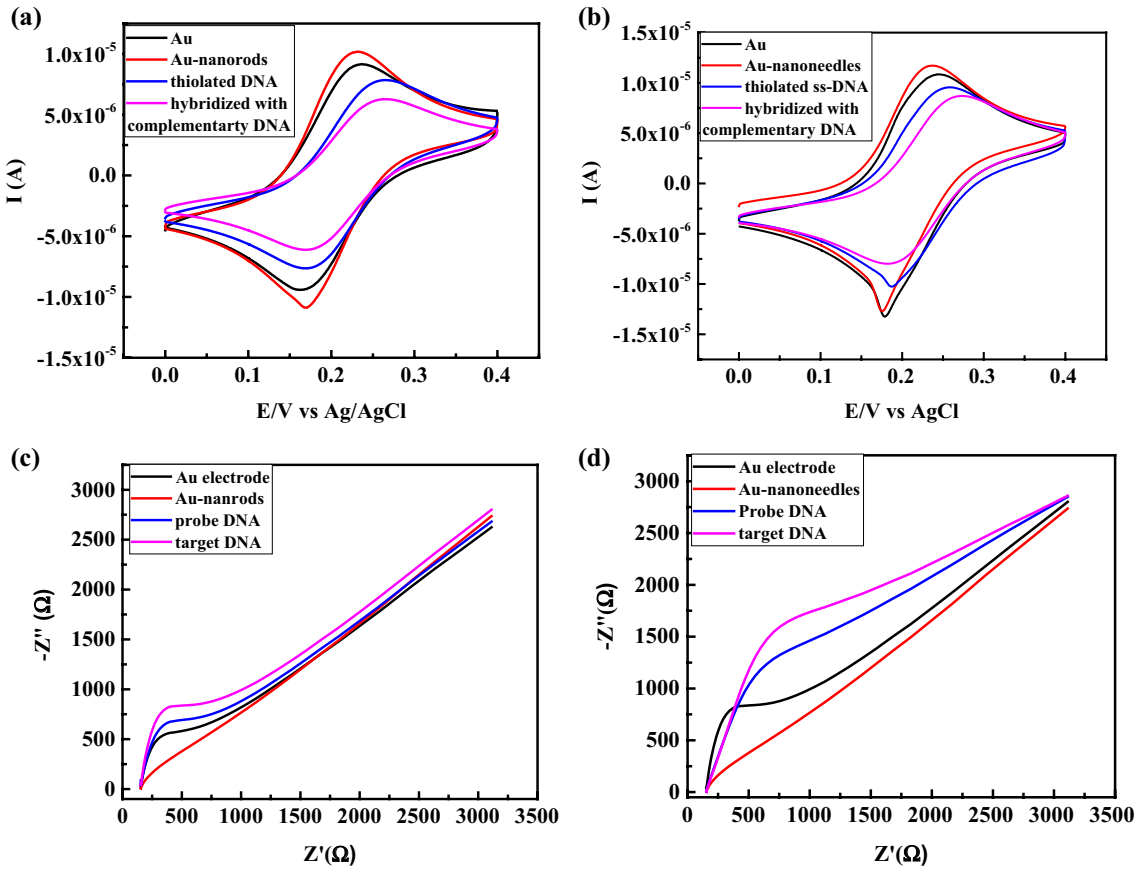

Fig. 5 Cyclic voltammogram measurement (**a**, **b**) and impedance plot (**c**, **d**) obtained for planar Au electrode (black line), the nanostructured electrode (red), the thiolated ss-DNA attachment (blue) and hybridization with complementary target DNA (pink) in 1 mM $[Ru(NH_3)_6]^{3+}$ in 0.1 M KCl solution for Au-nanaorod and Au-nanoneedle-modified electrodes

hybridization process. The results obtained were in good agreement with CV measurements shown in Fig. 5a, b.

DNA immobilization and hybridization

Differential pulse measurement of DNA biosensor

The differential pulse voltammetry (DPV) was performed to characterize the immobilization and hybridization process of DNA biosensor. The DPV measurements were performed in RuHex solution. The DPV curves obtained are shown in Fig. 6. The modification of electrode with probe DNA (thiolated ss-DNA) results in a peak current of about 2.29, 3.88 and 4.42 µA for planar gold electrode, Au-nanorod electrode, and Au-nanoneedle electrode, respectively, at a potential of about − 0.15 V. The hybridization of probe DNA with target complementary DNA gave a corresponding change in current of about 1.09, 2.43, and 3.41 µA. This showed that the target DNA hybridized with probe DNA. This change in current obtained was used to evaluate the hybridization efficiency of biosensor. The efficiency was calculated using formula $\Delta I/I_p$, where ΔI is the change in current observed before and after hybridization and I_p represents the current obtained after immobilization of probe DNA. The hybridization efficiency came out to be 49%, 61% and 79% for planar gold, Au-nanorods and Au-nanoneedles, respectively. The hybridization efficiency was greatly improved by depositing the nanostructures when compared with planar gold surface. It can also be observed that the Au-nanoneedle surface hybridization response was higher as compared to Au-nanorods. It also indicated that the immobilization amount of probe DNA on Au-nanoneedles was proportional to the surface area. This was due to the fact that the surface area enhanced by the deposition of Au-nanoneedles. Therefore, the probe DNA and hybridization efficiency improved significantly. Wang et al. has reported the hybridization efficiency of about 69% for DNA biosensor using gold nanoflowers (Wang et al. 2011). The biosensor prepared herein depicted an improved response for hybridization efficiency after deposition of Au-nanoneedles. An increase in current after hybridization with target complementary DNA showed a strong influence on the morphology of gold nanostructures.

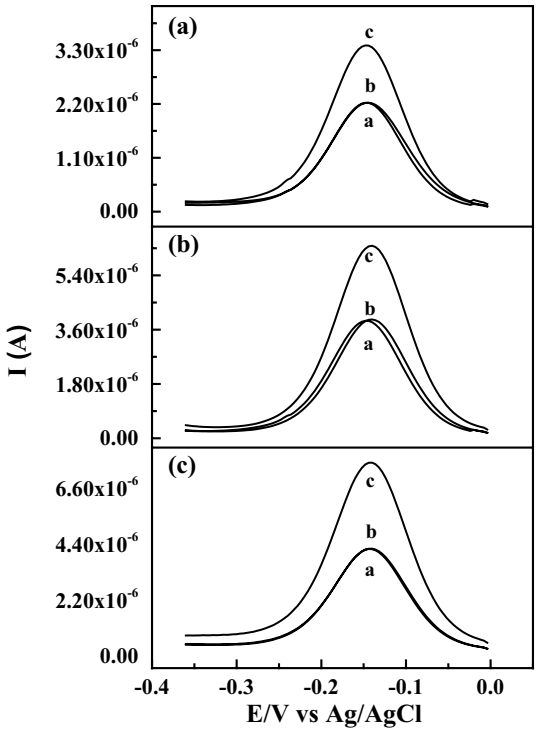

Fig. 6 Differential pulse voltammogram response of DNA biosensor with 1 mM $[Ru(NH_3)_6]^{3+}$ in 0.1 M KCl solution for **a** planar gold electrode, **b** electrode modified with Au-nanorods at potential of −0.08 V using 4 mM concentration of gold chloride and **c** Au nanoneedles at a potential of −0.08 V using 15 mM gold chloride concentration. The electrodes (a), (b) and (c) were obtained for thiolated ss-DNA, hybridization with non-complementary target DNA, and hybridization with complementary DNA

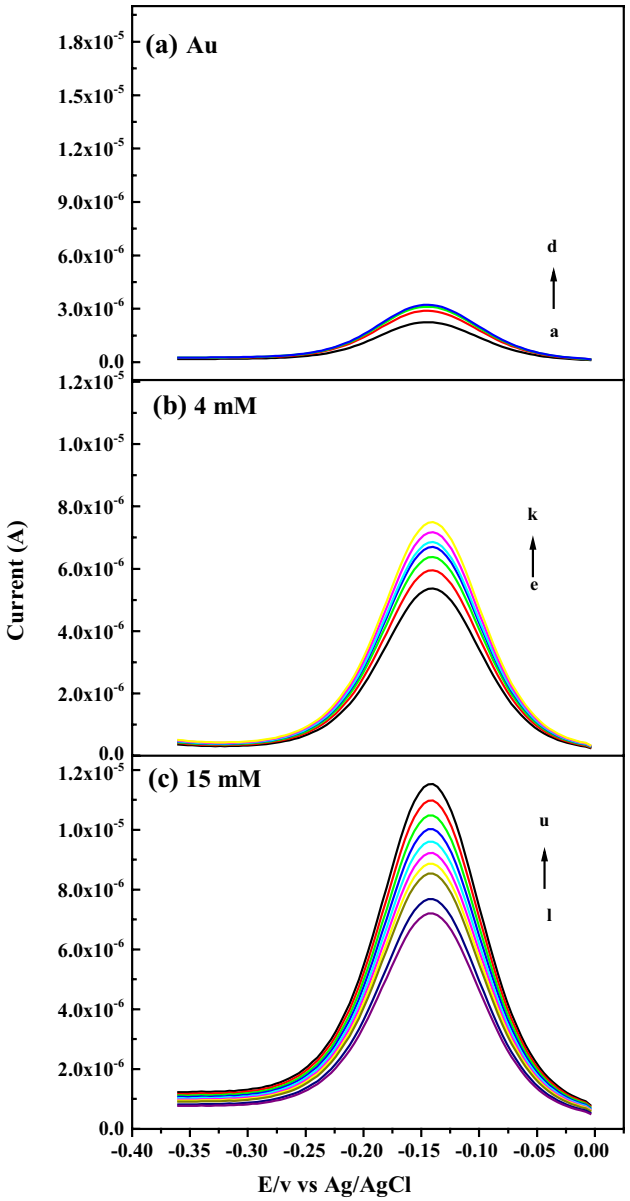

Fig. 7 The differential pulse voltammetry measurements. **a** Planar Au surface for different concentrations of target DNA ranges from 1 pM to 1 nM, **b** 4 mM gold chloride concentration, for concentration of target DNA ranges from 10 fM to 10 nM, and **c** 15 mM gold chloride concentration, for concentration of target DNA ranges from 0.2 fM to 10 nM

It can be seen that Au-nanoneedle electrode which exhibits larger surface area results in a highest increase in current after hybridization. This suggests that the amount of immobilization and hybridization increased with the surface area of the nanostructured electrode. Moreover, the morphology of gold nanostructure had a great effect on hybridization efficiency of DNA biosensor.

The controlled experiment was performed with the non-complementary DNA hybridized with probe DNA (Fig. 5, curve b) on plain Au, Au-nanorod and Au-nanoneedle surfaces. Almost the same response was obtained as was observed for probe DNA-modified surface. This represents a good selectivity of our DNA biosensor.

Detection limit for probe DNA

A change in the peak current before and after hybridization of probe and complementary DNA was used to evaluate the performance of DNA biosensor on plain Au, Au-nanorod and Au-nanoneedle modified electrodes for different concentration of target DNA. Each measurement was performed on three independent electrodes to measure a current for single concentration. The DPV peak current response increased with an increase in the probe DNA concentration as shown in Fig. 7 for concentration range from 10 pM to 10 nM, 10 fM to 10 nM and 0.2 fM to 10 nM for planar Au, Au-nanorods and Au-nanoneedles, respectively, whereas Li et al. (2011) produced a DNA biosensor with dynamic range of 1 fM to 1 nM with lower detection limit of 1 fM. The biosensor presented herein showed a dynamic concentration range of 0.2 fM–10 nM for Au-nanoneedles with

lower detection limit of 0.2 fM and it was much lower than the values reported in the literature. Moreover, a change in peak current (ΔI) obtained for different values of concentrations was plotted as shown in Fig. 8. It showed that the linear response was obtained to a log of concentration. The calibration curve for Au-nanoneedles was fitted with linear equation given by

$$I(\mu A) = 4.602\ \log\ (C)(M) + 17.56.$$

The fit gave the regression coefficient of 0.989 for Au-nanoneedles. In the equation, I is the current and C is the concentration of probe DNA. The parameters obtained for the performance of DNA biosensor are shown in Table 1. It can be seen that Au-nanoneedle-modified electrode can detect up to lower limit of 0.2 fM. It is quite low as compared to plain Au- and Au-nanorod-modified electrode. The detection limit obtained for plain Au surface was 13 pM. Therefore, the development of Au-nanoneedle by electrodeposition method led to enhanced sensitivity to several orders of magnitude as compared to the plain Au and Au-nanorod electrode.

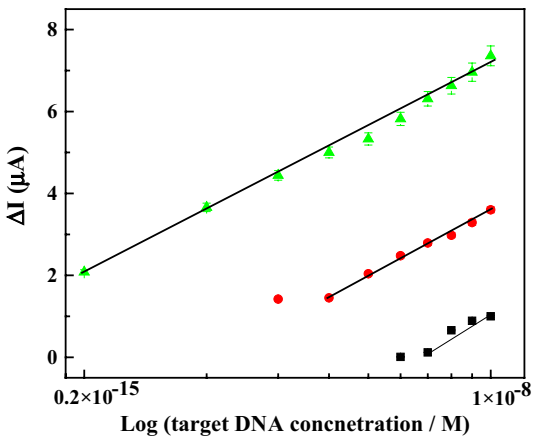

Fig. 8 Change in current obtained from differential pulse voltammetry as a function of logarithm of target DNA concentration for planar electrode (black, target DNA concentration from 1 pM to 1 nM), 4 mM concentration (red, target DNA concentration from 10 fM to 10 nM) and 15 mM concentration (green, target DNA concentration from 0.2 fM to 10 nM). Three different electrodes were used for the fabrication of biosensor and measurements were repeated five times on each single planar Au, Au-nanorod and Au-nanoneedle-modified electrode

Reproducibility and stability of Au-nanoneedle DNA biosensor

For clinical diagnosis, it is very important to monitor the reproducibility of the fabricated DNA biosensor. For this purpose, three different electrodes were used for the fabrication of biosensor and measurements were repeated five times on each single Au-nanoneedle-modified electrode at a target DNA concentration of 1 fM. The fabricated DNA biosensor gave an average peak current of 8.5 μA with standard deviation of 4%. The electrode to electrode reproducibility was also monitored. These modified electrodes showed a coefficient of variation of 3.4%. The results showed that the response of fabricated biosensor on different electrodes has similar behaviour.

The stability of Au-nanoneedle DNA biosensor was also investigated. The probe DNA-modified electrodes were stored in refrigerator at 4 °C for 3 weeks. The DPV measurements were performed after its hybridization with target DNA concentration of 1 fM. The DPV measurements revealed that the fabricated DNA biosensor retained almost 89% of its original current value. It showed a good stability of prepared DNA biosensor.

Conclusion

This study presents a simple one-step electrochemical method which was employed to deposit Au-nanostructure for sensitive detection of short DNA sequence. The developed Au-nanorods and Au-nanoneedles enhanced the surface to 2.7 and 3.6 times as compared to planar gold surface. The Au-nanoneedle surface increased the immobilized amount of probe DNA which results in an increase in the hybridization of target DNA. The fabricated DNA biosensor showed the detection limit of 1 pM, 1 fM and 0.2 fM for planar, Au-nanorods and Au-nanoneedles, respectively. The detection limit has improved several orders of magnitude as compared to planar Au surface. Moreover, the prepared biosensor is

Table 1 The parameters concentration range, limit of detection (LOD), correlation coefficient and sensitivity were evaluated to examine the detection performance of planar, Au-nanorod-, and Au-nanoneedle-modified electrodes

	Concentration range	Sensitivity ($\mu A\ mol^{-1}\ L$)	Intercept (μA)	r^2	LOD
Planar Au	0.2 fM to 10 nM	2.75 ± 0.14	− 2.73 ± 0.32	0.968	13 pmol L^{-1}
Au-nanorods	10 fM to 10 nM	3.37 ± 0.25	− 5.69 ± 0.23	0.966	10 fmol L^{-1}
Au-nanoneedles	10 pM to 10 nM	4.06 ± 0.32	1.75 ± 0.49	0.989	0.2 fmol L^{-1}

expected to show an excellent response for different applications such as protein and enzyme detection.

Acknowledgements This work was supported by the Higher Education Commission, Pakistan (HEC) development grant for "National Research Program for Universities (NRPU)" through Project no. 10109/Federal/NRPU/R&D/HEC/2017.

Compliance with ethical standards

Conflict of interest The authors declare no conflicts of interest.

References

Alim S, Vejayan J, Yusoff MM, Kafi AKM (2018) Recent uses of carbon nanotubes and gold nanoparticles in electrochemistry with application in biosensing: a review. Biosens Bioelectron 121:125–136. https://doi.org/10.1016/j.bios.2018.08.051

Elahi N, Kamali M, Baghersad MH (2018) Recent biomedical applications of gold nanoparticles: a review. Talanta 184:537–556. https://doi.org/10.1016/j.talanta.2018.02.088

Fojta M, Daňhel A, Havran L, Vyskočil V (2016) Recent progress in electrochemical sensors and assays for DNA damage and repair. Trans Trends Anal Chem 79:160–167. https://doi.org/10.1016/j.trac.2015.11.018

Fortunati S, Rozzi A, Curti F, Giannetto M, Corradini R, Careri M (2019) Novel amperometric genosensor based on peptide nucleic acid (PNA) probes immobilized on carbon nanotubes-screen printed electrodes for the determination of trace levels of non-amplified DNA in genetically modified (GM) soy. Biosens Bioelectron 129:7–14. https://doi.org/10.3390/s19030588

Fu X, Xu K, Feng X (2016) Synthesis of sunflower-like gold nanostructure and its application in the electrochemical immunoassay using nanogold-triggered hydrogen evolution reaction. Anal Methods 8:958–961. https://doi.org/10.1039/C5AY03174E

Hajkova A, Barek J, Vyskocil V (2015) Voltammetric determination of 2-aminofluoren-9-one and investigation of its interaction with DNA on a glassy carbon electrode. Electroanalysis 27:101–110. https://doi.org/10.1002/elan.201400427

Hajkova A, Barek J, Vyskocil V (2017) Electrochemical DNA biosensor for detection of DNA damage induced by hydroxyl radicals. Bioelectrochemistry 116:1–9. https://doi.org/10.1016/j.bioelechem.2017.02.003

Hamelin A (1996) Cyclic voltammetry at gold single-crystal surfaces. Part 1. Behaviour at low-index faces. J Electroanal Chem 407:1–11. https://doi.org/10.1016/0022-0728(95)04499-X

Han X, Fang X, Shi A, Wang J, Zhang Y (2013) An electrochemical DNA biosensor based on gold nanorods decorated graphene oxide sheets for sensing platform. Anal Biochem 443:117–123. https://doi.org/10.1016/j.ab.2013.08.027

Hlavata L, Benikova K, Vyskocil V, Labuda J (2012) Evaluation of damage to DNA induced by UV-C radiation and chemical agents using electrochemical biosensor based on low molecular weight DNA and screen-printed carbon electrode. Electrochim Acta 71:134–139. https://doi.org/10.1016/j.electacta.2012.03.119

Huang K, Liu Y, Wang HB, Wang Y (2014) A sensitive electrochemical DNA biosensor based on silver nanoparticles-polydopamine@graphene composite. Electrochim Acta 118:130–137. https://doi.org/10.1016/j.electacta.2013.12.019

Huang Y, Xu J, Liu J, Wang X, Chen B (2017) Disease-related detection with electrochemical biosensors: a review sensors 1:2375–2405. https://doi.org/10.3390/s17102375

Hun X, Liu B, Meng Y (2017) Ultrasensitive chemiluminescence assay for the lung cancer biomarker cytokeratin 21-1 via a dual amplification scheme based on the use of encoded gold nanoparticles and a toehold-mediated strand displacement reaction. Microchim Acta 184:3953–3959. https://doi.org/10.1007/s00604-017-2430-x

Janegitz BC, Cancino J, Zucolotto V (2014) Disposable biosensors for clinical diagnosis. J Nanosci Nanotechnol 14:378–389. https://doi.org/10.1166/jnn.2014.9234

Jiang H, Lee EC (2018) Highly selective, reusable electrochemical impedimetric DNA sensors based on carbon nanotube/polymer composite electrode without surface modification. Biosens Bioelectron 118:6–22. https://doi.org/10.1016/j.bios.2018.07.037

Kokkinos C, Prodromidis M, Economou A, Petrou P, Kakabakos S (2015) Quantum dot-based electrochemical DNA biosensor using a screen-printed graphite surface with embedded bismuth precursor. Electrochem Commun 60:47–51. https://doi.org/10.1016/j.elecom.2015.08.006

Lee YHL, Zhang Y, Hsing IM (2017) Kinetically-enhanced DNA detection via multiple-pass exonuclease III-aided target recycling. Analyst 142:4782–4787. https://doi.org/10.1039/c7an01423f

Li F, Han X, Liu S (2011) Development of an electrochemical DNA biosensor with a high sensitivity of fM by dendritic gold nanostructure modified electrode. Biosens Bioelectron 26:2619–2625. https://doi.org/10.1016/j.bios.2010.11.020

Li GR, Xu H, Lu XF, Feng JX, Tong YX, Su CY (2013) Electrochemical synthesis of nanostructured materials for electrochemical energy conversion and storage. Nanoscale 5:4056–4069. https://doi.org/10.1039/c3nr00607g

Liu S, Liu J, Wang L, Zhao F (2010) Development of electrochemical DNA biosensor based on gold nanoparticle modified electrode by electroless deposition. Bioelectrochemistry 79:37–42. https://doi.org/10.1016/j.bioelechem.2009.10.005

Mahshid S, Mepham AH, Mahshid SS, Burgess IB, Saberi Safaei T, Sargent EH, Kelley SO (2016) Mechanistic control of the growth of three-dimensional gold sensors. J Phys Chem C 120:21123–21132. https://doi.org/10.1021/acs.jpcc.6b05158

Mogha NK, Sahu V, Sharma RK, Masram DT (2018) Reduced graphene oxide nanoribbon immobilized gold nanoparticle based electrochemical DNA biosensor for the detection of *Mycobacterium tuberculosis*. J Mater Chem B 6:5181–5187. https://doi.org/10.1039/c8tb01604f

Mohammed AM, Rahim RA, Ibraheem IJ, Loong FK, Hisham H, Hashim U, Al-Douri Y (2014) Application of gold nanoparticles for electrochemical DNA biosensor. J Nanomater 2014:1–7. https://doi.org/10.1155/2014/683460

Nakano S, Miyoshi D, Sugimoto N (2014) Effects of molecular crowding on the structures, interactions, and functions of nucleic acids. Chem Rev 114:2733–2758. https://doi.org/10.1021/cr400113m

Park BW, Yoon DY, Kim DS (2011) Formation and modification of a binary self-assembled monolayer on a nano-structured gold electrode and its structural characterization by electrochemical impedance spectroscopy. J Electroanal Chem 661:329–335. https://doi.org/10.1016/j.jelechem.2011.08.013

Povedano E, Eloy P, Eva V, Víctor RM, Rebeca MT, María P, Rodrigo B, Pablo SS, Alberto P, Marta M, David H, Susana C, José MP (2018) Electrochemical affinity biosensors for fast detection of gene-specific methylations with no need for bisulfite and amplification treatments. Sci Rep 8:6418. https://doi.org/10.1038/s41598-018-24902-1

Rasheed PA, Sandhyarani N (2017) Carbon nanostructures as immobilization platform for DNA: a review on current progress in electrochemical DNA sensors. Biosens Bioelectron 97:226–237. https://doi.org/10.1016/j.bios.2017.06.001

Saeed AA, Sanchez JLA, O'Sullivan CK, Abbas MN (2017) DNA biosensors based on gold nanoparticles-modified graphene oxide for the detection of breast cancer biomarkers for early diagnosis.

Bioelectrochemistry 118:91–99. https://doi.org/10.1016/j.bioelechem.2017.07.002

Sohrabi N, Valizadeh A, Farkhani SM, Akbarzadeh A (2016) Basics of DNA biosensors and cancer diagnosis. Artif Cell Nanomed Biotechnol 44:654–663. https://doi.org/10.3109/21691401.2014.976707

Soleymani L, Fang Z, Sargent EH, Kelley SO (2009) Programming the detection limits of biosensors through controlled nanostructuring. Nat Nanotechnol 4:844–848. https://doi.org/10.1038/nnano.2009.276

Soleymani L, Fang Z, Lam B, Bin X, Vasilyeva E, Ross AJ, Sargent EH, Kelley SO (2011) Hierarchical nanotextured microelectrodes overcome the molecular transport barrier to achieve rapid direct bacterial detection. ACS Nano 5:3360–3366. https://doi.org/10.1021/nn200586s

Sun X, Dong S, Wang E (2004) Large-scale synthesis of micrometer-scale single-crystalline Au plates of nanometer thickness by a wet-chemical route. Angew Chem 43:6360–6363. https://doi.org/10.1002/anie.200461013

Tan LH, Xing H, Lu Y (2014) DNA as a powerful tool for morphology control, spatial positioning, and dynamic assembly of nanoparticles. Acc Chem Res 47:1881–1890. https://doi.org/10.1021/ar500081k

Tian Y, Liu H, Zhao G, Tatsuma T (2006) Shape-controlled electrodeposition of gold nanostructures. J Phys Chem B 110:23478–23481. https://doi.org/10.1021/jp065292q

Veselinovic J, Li Z, Daggumati P, Seker E (2018) Electrically guided DNA immobilization and multiplexed DNA detection with nanoporous gold electrodes. Nanomaterials 8:351–359. https://doi.org/10.3390/nano8050351

Wang L, Chen X, Wang X, Han X, Liu S, Zhao C (2011) Electrochemical synthesis of gold nanostructure modified electrode and its development in electrochemical DNA biosensor. Biosens Bioelectron 30:151–157. https://doi.org/10.1016/j.bios.2011.09.003

Zhong G, Liu A, Xu X, Sun Z, Chen J, Wang K, Liu Q, Lin X, Lin J (2012) Detection of femtomolar level osteosarcoma-related gene via a chronocoulometric DNA biosensor based on nanostructure gold electrode. Int J Nanomed 7:527–536. https://doi.org/10.2147/IJN.S27794